Internal and near nozzle flow characteristics in an enlarged model of an outwards opening pintle-type gasoline injector

Abo-Serie, E., Nouri, J. M., Marchi, A., Mitroglou, N. & Arcoumanis, C.

Internal and near nozzle flow characteristics in an enlarged model of an outwards opening pintle-type gasoline injector

To cite this article: J M Nouri *et al* 2007 *J. Phys.: Conf. Ser.* **85** 012035

View the article online for updates and enhancements.

IOP ebooks™

Bringing you innovative digital publishing with leading voices to create your essential collection of books in STEM research.

Start exploring the collection - download the first chapter of every title for free.

Internal and near nozzle flow characteristics in an enlarged model of an outwards opening pintle-type gasoline injector

J. M. Nouri, E. Abo-Serie, A. Marchi, N. Mitroglou and C. Arcoumanis

Centre for Energy and the Environment, School of Engineering and Mathematical Sciences, The City University, Northampton Square, London, EC1V OHB, UK

Abstract. The internal nozzle and near the nozzle exit flows of an enlarged transparent model of an outwards opening injector were investigated for different flow rates and needle lifts under steady state flow conditions. A high resolution CCD camera, high speed video camera and an LDV system were employed to visualize the nozzle flow and quantify the tangential velocity characteristics. The images of the internal flow between the valve seat and the square cross-section end of the needle guide revealed the presence of four separated jet flows and four pairs of counter-rotating vortices with each pair bounded in-between two adjacent jets. The counter-rotating vortices are highly unstable with a circumferential oscillatory motion which was transmitted to the spray outside the nozzle with almost the same frequency. The dominant circumferential frequencies at the nozzle exit were identified by FFT analysis of the tangential velocities. A linear relationship exists between the dominant frequencies and the flow Reynolds number based on injection velocity and needle lift. Magnified images of the flow just outside the nozzle exit showed formation of interconnecting streamwise strings on the liquid film as soon as it emerges from the annular exit passage. The interspacing between the strings was found to be linearly related to injection velocity and almost independent of the needle lift.

1. Introduction

Direct injection of gasoline into the engine cylinder is regarded as one of the main strategies to improve the combustion efficiency of spark ignition engines and represents a promising approach to meet the overall target for improvement of fuel economy and reduction of CO_2 emissions [1]. To achieve this target, higher compression ratio is applied together with a lean combustion strategy during part load operation (injection during late compression stroke) using a stratified charge. The success of such a strategy depends on a suitable injector that is able to produce a stable spray at both full load and part load operations, particularly if the spray-guided approach is adopted for low loads [2].

The outwards opening injection nozzle is one of the most important components in the direct injection spark ignition (DISI) spray-guided system. The spray pattern from this type of injector has a hollow cone spray structure similar to the swirl type atomiser. Previous work on this injector is rather limited and an early study [3] showed that the generated spray does not contain the poorly atomized pre-spray present in swirl injectors [4]. Moreover it offers flexibility since the initial liquid film

thickness is directly controlled by the injector needle stroke rather than the angular velocity of the swirling fuel. Another advantage of this injector is the flushing out of any deposits accumulated on the tip of the injector. The main disadvantage of this injector, on the other hand, is the relatively high degree of spray-to-spray variations. It is crucial for spray-guided combustion systems to produce a stable spray with minimum variations not only at the same cylinder conditions but also under different engine loads and speeds since in spray-guided systems the spark plug and injector are located close to each other and any spray deviation from its targeted spark plug location can lead to misfire.

Designing an injector to produce a spray with specified characteristics is always a very time consuming task, and in most cases, it is based on extensive measurements on a trial and error basis due to the limited information about the flow conditions at the nozzle exit and the related fuel atomisation process. The present injector represents an alternative option for DISI engines to the multi-hole injectors [5].

Early images of the spray from this outwards opening injector showed small spray-to-spray variations and a string-type structure originating at the nozzle exit. This structure has been studied before [6,7] and it has been confirmed to be the result of the interaction between the airflow and the emerging annular liquid film. However, most of these studies were limited to low injection velocities and relatively high air cross flow velocities. Streamwise ligaments were observed very close to the nozzle exit as the liquid velocity increases and spanwise waves were developed on top of the streamwise ligaments which, through growth, gave rise to distorted waves [8]. The streamwise frequency of these ligaments was directly related to the air and liquid velocities. The enlarged injector was operating at similar injection Reynolds numbers to previous studies but with no air cross-flow.

The objective of the present work was to investigate the internal nozzle flow characteristics and, in particular the flow strings formation near the nozzle exit in an enlarged model (23.3:1) of the prototype injector which was manufactured from Perspex to provide full optical access. The internal flow was visualised with a continuous light source, a high resolution CCD camera and a high speed video recorder and some details of the tangential velocity were measured with a laser Doppler velocimeter (LDV). The following sections describe, in turn, the experimental arrangement and instrumentation, the results and their implications and provide a summary of the most important conclusions.

2. Experimental set up and large scale models

A large-scale nozzle (23.3:1) has been manufactured from plexiglass (Perspex) simulating the outwards opening DISI injector as shown in Fig. 1. The model was designed based on dynamic similarity with that of the real injector at the nozzle exit. The flow circuit through the enlarged nozzle injector was operated under steady flow conditions by fixing the needle position. The nozzle internal flow and the near the nozzle exit spray were visualized using a high resolution CCD camera 1200x1055 pixels and a high speed video camera with 18000 fps to allow capturing the structure of the flow and to record its real time variation.

An LDV system was also employed to measure the circumferential flow velocities at the nozzle exit, as shown in Fig. 1. Since it was not possible to measure this flow velocity component at the nozzle exit for the case of water injected into air, due to the water surface shape dynamics causing laser beam multiple scattering, the water jet was injected into a closed plexiglass chamber full of water which allowed focusing the control volume onto the water jet. It should be stressed, however, that the flow velocity measured in the chamber may not be equal to the jet free surface velocity (when water is injected into air) because of the different viscous effect. Nevertheless, the velocity measurements in the vicinity of the nozzle exit are less affected and can provide useful information in an attempt to explain the mechanism of formation of the strings filaments.

2.1 OPERATING CONDITIONS

The water used in the system was injected with a velocity comparable to that in the actual injector in order to maintain the same Reynolds number, Re, which was calculated as follows:

$$\mathrm{Re} = \frac{2 \cdot \rho_f \cdot U_{inj} \cdot Lift \cdot \sin \alpha}{\mu_f}$$

where $\quad U_{inj} = \dfrac{\dot{Q}}{A}$.

and ρ_f and μ_f are the fuel density and dynamic viscosity, respectively, and the geometric symbols are shown in Fig. 2. For a given flow rate ($\dot{Q}$) and flow area at the channel exit (A), the mean injection velocity and Reynolds number under steady flow conditions can be calculated. Table 1 shows the operating conditions for three flow rates in the enlarged model and their corresponding values in the real size injector.
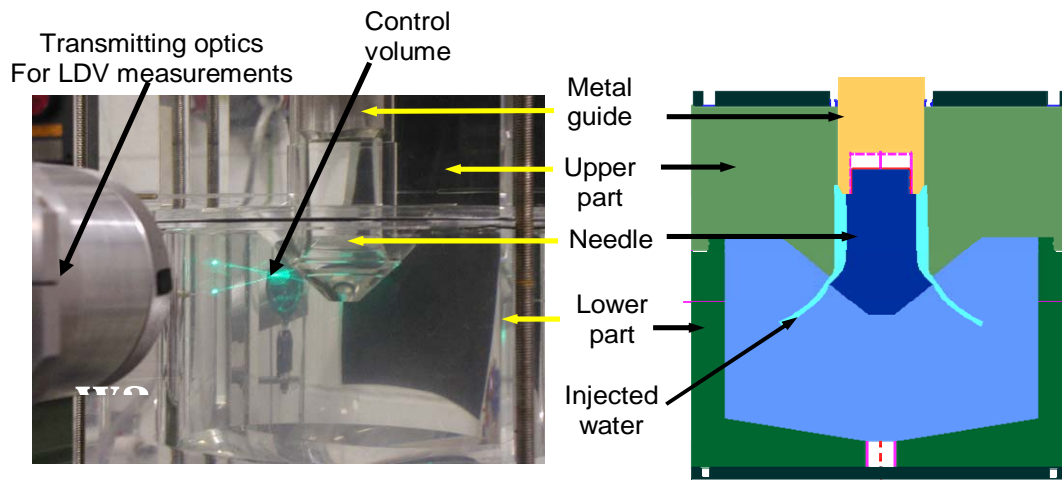
Figure 1 Schematic showing the main components of the large-scale nozzle model

Needle Lift			Flow Rate		Uinj	
Model [mm]	Real [mm]	Re	Model [l/s]	Real [g/s]	Model [m/s]	Real [m/s]
0.575	0.025	6513	0.95	11.9	8.8	88
0.928	0.040	6526	0.95	11.9	5.5	54
0.575	0.025	11793	1.72	21.5	16.0	159
0.928	0.040	11815	1.72	21.5	9.9	99
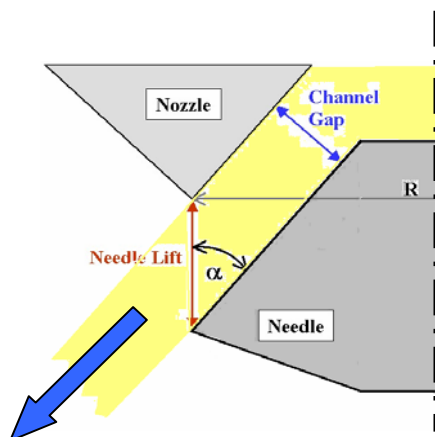
Figure 2 Geometry of the needle and its seat.

Table 1 Operating conditions and the corresponding values for the real size nozzle.

3. Results and discussion

The results of the internal-nozzle flow are presented first, followed by the flow results near the nozzle exit and the LDV results.

3.1 Internal-nozzle flow characteristics

Flow visualization

After assembling the large-scale injector, a preliminary test was carried out using water as the working fluid to make sure that all components of the system were working properly and the results were satisfactory.

The development of cavitation was first examined under similar operating conditions to those in the real size nozzle. The results confirmed that no cavitation, either geometric or dynamic, was initiated under all operating conditions in the nozzle seat region.
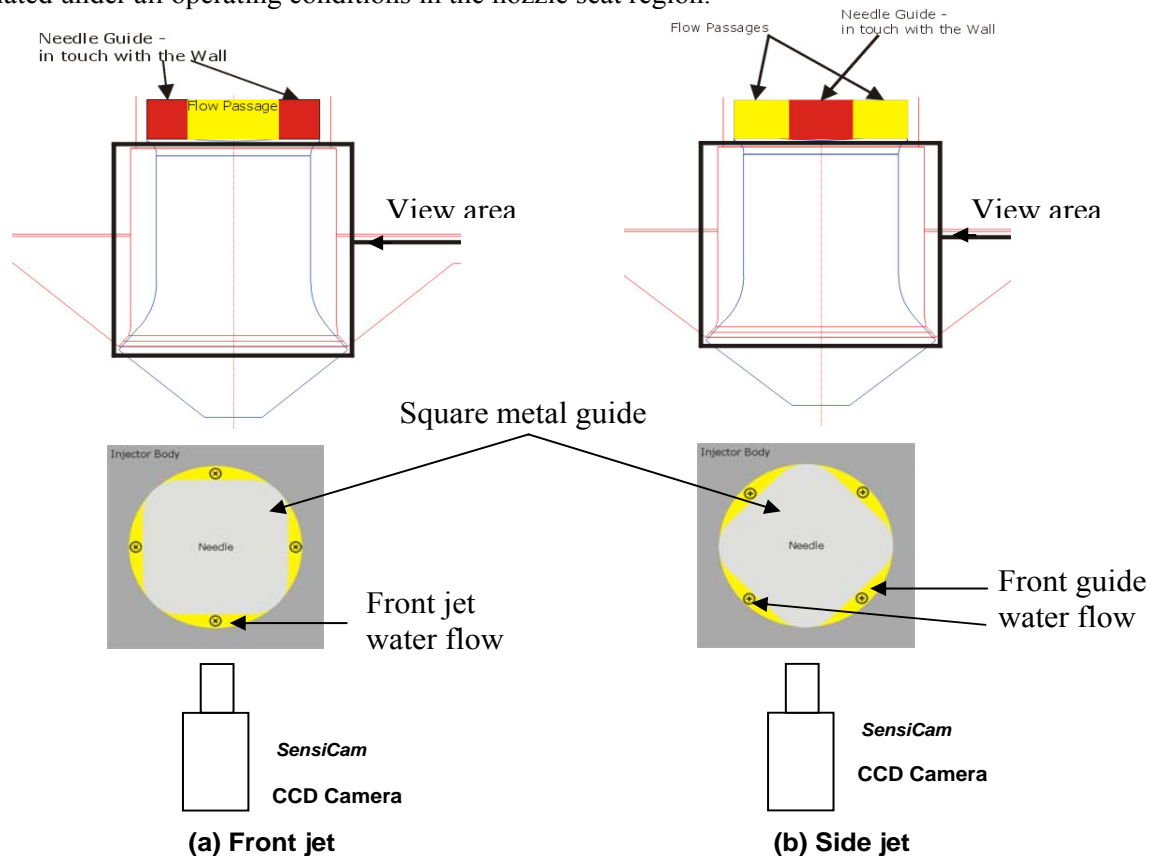

Figure 3 Schematic showing the camera location for flow visualisation downstream of the square-section needle guide and upstream of the valve seat for both front and side jet water flows.

In order to trace the flow downstream of the square-section needle guide and upstream of the valve seat, a small amount of air has been introduced into the main delivery pipe through a fine needle with a diameter of 0.15 mm. The formed small air bubbles follow faithfully the water flow streamlines and could be visualised due to the difference in the refractive index between air and water. Although special attention has been paid to reduce the air bubble sizes by changing the needle size and the amount of injected air, it was not possible to have small air bubbles at low flow rates. However, images obtained at both low and high flow rates showed similar flow patterns. This method proved

successful to describe the mean flow pattern but not accurate enough to provide quantitative data for model validation. The latter was possible through a 1-D LDV measurements to be presented later.

The flow patterns between the valve seat and the square-section needle guide were visualised using a high resolution CCD camera for the case of the camera facing the jet (front jet view) and from the side of the two jets (front guide view), as shown in Fig. 3. The square needle guide has four flow passages and four rounded corners which are in touch with the needle casing (cartridge). In the imaged flow areas, four liquid jets originating from the square-section needle guide are interacting with each other to form a complex and unsteady vortical structure in the region between the needle guide and the needle seat, as shown in Fig. 4; the arrows superimposed on the images indicate the direction of the flow.

The presence of counter-rotating recirculation zones is clearly evident from the side jet images of Fig. 4a; these random images indicate that the flow is highly unstable with the vortical interaction causing an upwards jet that is swinging from left to right. Figure 4b shows the front jet images with the main jet in the centre and two main vortices on either side. Although the main jet seems to be more stable and its centre coincides with the nozzle centreline, the surrounding vortices appeared to be moving in a random fashion.
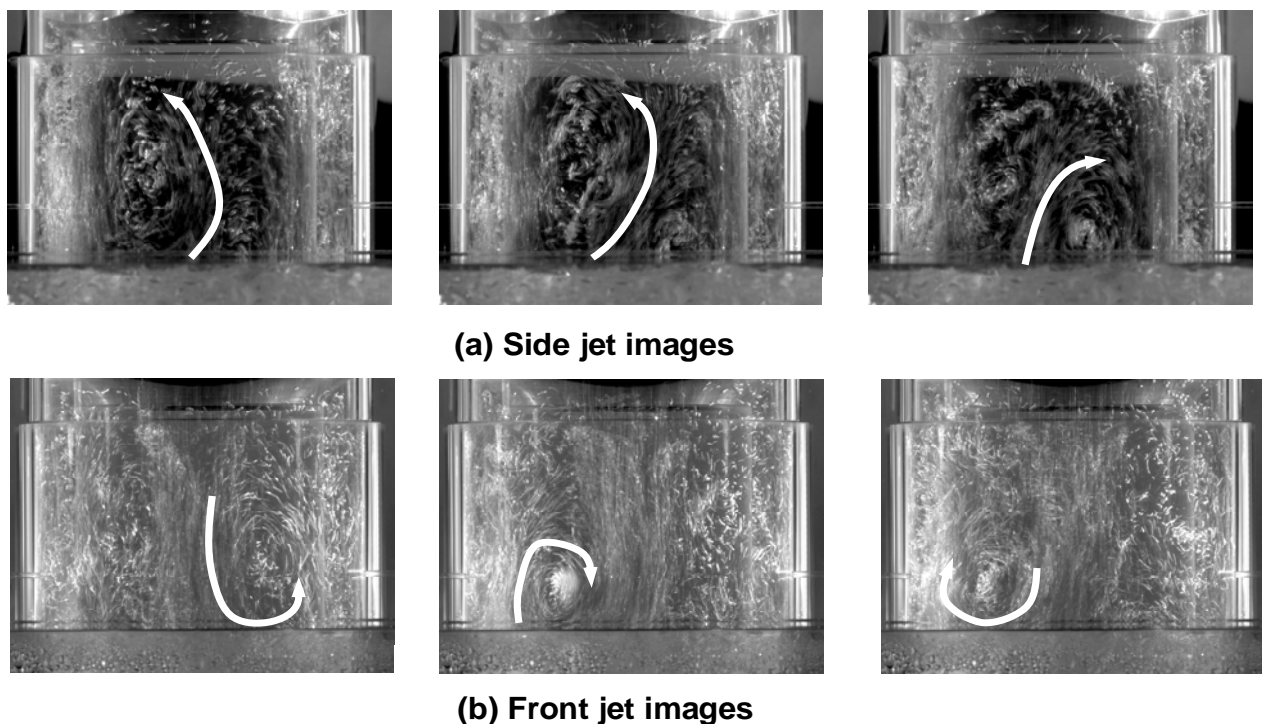

(a) Side jet images

(b) Front jet images

Figure 4 Images showing the flow downstream of the square-section needle guide and upstream of the valve seat for both front and side jet water flows: needle lift=0.57 mm and flow rate 1.7 l/s.

Overall, the flow pattern between the valve seat and the square-section needle guide comprised four separated jets originating from the square cross-section needle guide and four pairs of counter-rotating vortices with each pair bounded in-between two adjacent jets. The counter-rotating vortices are highly unstable and are expected to affect the spray stability outside the nozzle; this instability is clearly evident in video recording of the flow. A schematic description of the flow pattern in this region is shown in Fig. 5 which reveals how the two adjacent jet flows are meeting each other above the valve seat. This meeting point (M in Fig. 5) of the two jets is as unstable as the two vortices above it.

The instability is evident in the form of oscillations in both the longitudinal (along the axis of injector) and circumferential directions; closer observation of the spray revealed that the longitudinal mode of oscillation was suppressed as the flow passed through the narrow valve seat. On the other hand, the circumferential flow oscillation was transmitted by the liquid flow through the valve seat into the spray forcing it to oscillate. Simultaneous recording of the liquid spray and the internal flow (counter-rotating vortices) confirmed that both were oscillating with the same frequency. A similar flow pattern and instability were also observed at all flow rates and valve lifts examined, from full to the smallest lift of 0.32 mm (equivalent to 14μm in the real size). Changing these parameters, affects only the velocity of the liquid but not the flow pattern.
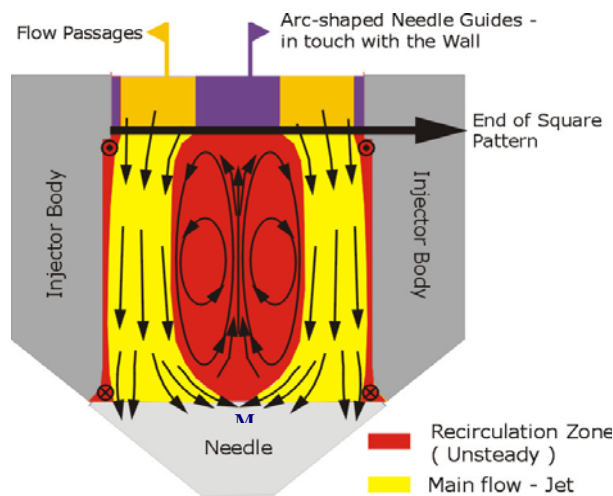

Figure 5 Schematic flow pattern between the valve seat and the square-section needle guide.

3.2 Nozzle exit frequency and LDV measurements

To further investigate the link between the internal nozzle flow and the flow downstream the nozzle exit, the tangential velocity of the exit liquid film was measured at different axial locations (see Fig. 6) using an LDV system. In general, the magnitude of the mean tangential velocities is close to zero, as shown in Fig. 7. However, the temporal variation of the instantaneous velocity showed clearly that the flow in the circumferential direction oscillates around the zero value; by applying FFT it was possible to estimate the dominant frequencies of the oscillatory flow.
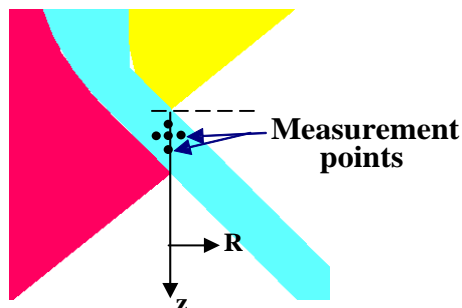

Figure 6 Control volume locations for LDV tangential velocity measurements
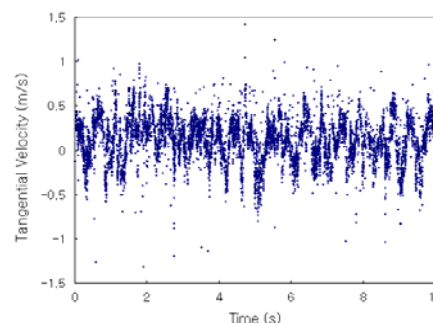

Figure 7 Tangential velocity measurements within the liquid jet at the nozzle exit.

The FFT analysis (Fig. 8) showed that there are three dominant frequencies; one of these frequencies is always the dominant one. Moving the control volume vertically along the exit gap did

not change the dominant frequency; however, this was not the case when moving the control volume horizontally. By moving the measurement point inside the gap closer to the nozzle axis, the most dominant frequency shifted towards lower values. Nevertheless, the values of the three dominant frequencies are relatively low compared with the break-up frequency and their values are directly related to the flow oscillations occurring inside and outside the nozzle exit as mentioned previously. Although the control volume was considerably long and the positional uncertainty was estimated to be 0.5 mm, it was clear that the higher frequency becomes more dominant when moving the control volume away from the nozzle.
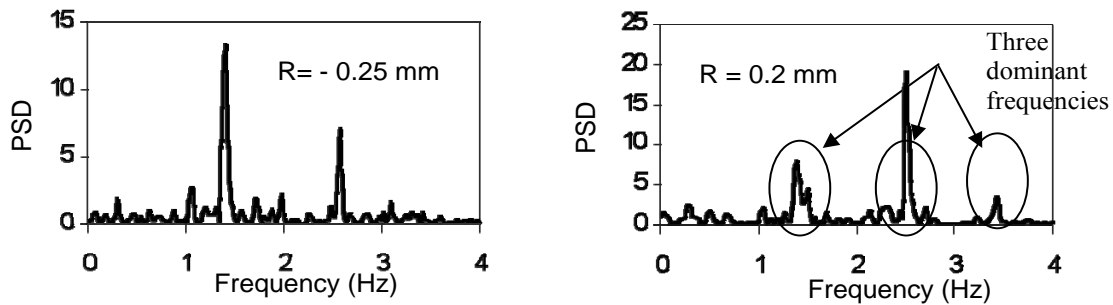

Figure 8 Dominant frequencies of the flow at two horizontal locations, Q=0.7l/s, lift= 0.93mm.

In order to study the effect of the flow rate on the dominant frequencies, these frequencies were estimated and plotted for different flow rates. A linear relationship was found which means that the dominant frequencies are directly proportional to the flow rates, as shown in Fig. 9(a). Since the flow rate is calculated based on the injection velocity and the needle lift, it was necessary to investigate which of these two parameters is more pronounced. A linear relationship was found between either the injection velocity or needle lift and the dominant frequencies which highlights the effect of the Reynolds number. The results are presented in Fig. 9(b) which shows clearly the existence of a linear relationship, although it has to be stressed that the effect of viscosity is not examined. Since the Reynolds number was very similar between the real and the large scale model, it can be argued that they have similar values of frequency. Further investigation in the real size injector is needed to confirm this finding.
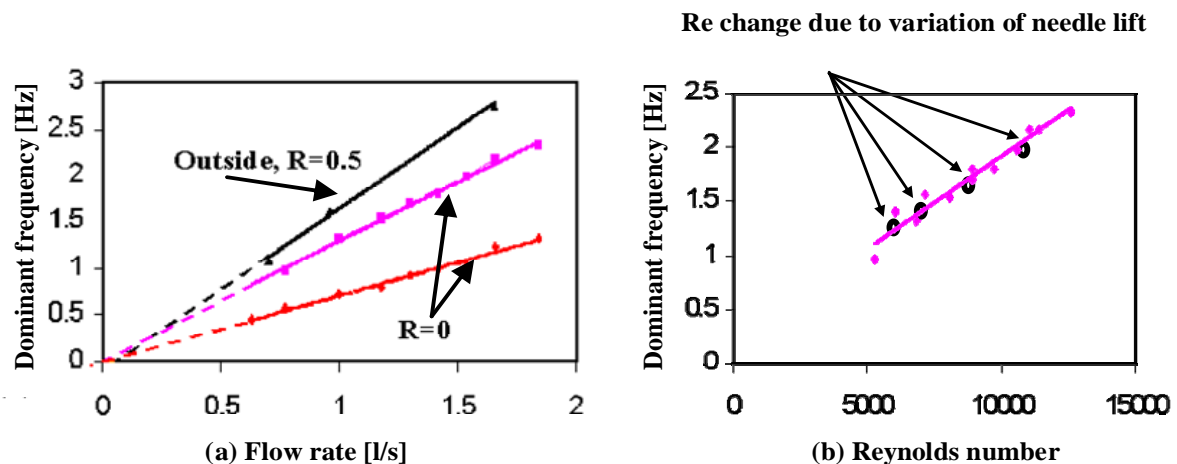

(a) Flow rate [l/s]   (b) Reynolds number

Figure 9 Variation of dominant frequency with flow rate and Reynolds number.

3.3 Flow filaments formation characteristics at the nozzle exit

An example of the flow close to the nozzle exit is shown in Fig. 10 where the overall and close-up images of the liquid film are presented. A wavy structure along the circumferential direction is clearly evident, characterized by streamwise interconnecting filaments dominating the liquid film surface. The existence of these waves was dependent on injection velocity so that at very low flow rates the liquid film surface was very smooth with a tulip shape and no evidence of filaments. In general, over the operating flow rates that give a similar range of Reynolds numbers to the real size injector, the string structure was clearly evident. The wavelength (string spacing) seems to be relatively small compared to the nozzle diameter, but comparable to the gap of the nozzle and within the atomization length scale range.
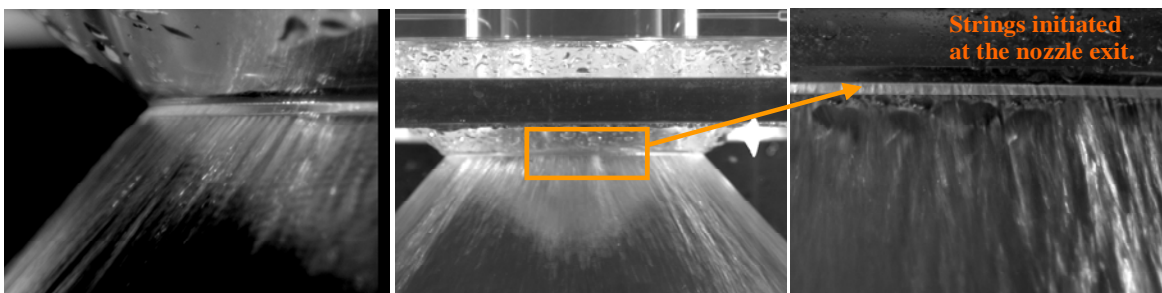

Figure 10 Images of the water spray with filaments structure on the surface of the liquid film close to the nozzle exit.

The observation of the strings structure in Fig. 10 was quite important since a similar structure was observed in the real size injector, as shown in Fig. 11. The fact that the large-scale model exhibits a similar behaviour implies that these strings do not come from surface roughness effects at the valve seat since the surface roughness at the seat of the model injector is marginal compared to the real size due to the different manufacturing process and the different material used in the enlarged model (plexiglass) which ensured a much smoother surface finish.
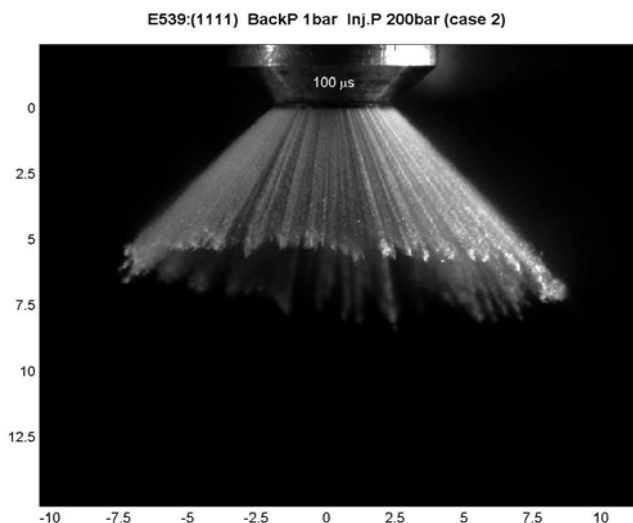

Figure 11 An image of the spray from a real size injector at 0.1 ms after the start of injection at an injection pressure of 200 bar and atmospheric back pressure.

In order to find the origin of these waves, the CCD camera was focused on the flow at the nozzle exit, in particular in the narrow gap between the needle and its seat. By using back lighting illumination and zoom lens to magnify the flow structure, it was possible to visualise clearly the filaments as shown in the image of Fig. 12. The magnified image of the flow near the nozzle exit clearly shows the filaments structure and their numbers can easily be counted over the imaging area of 6 mm long. With this set up a series of tests were carried out in order to investigate the effect of injection velocity and valve lift on filaments formation.
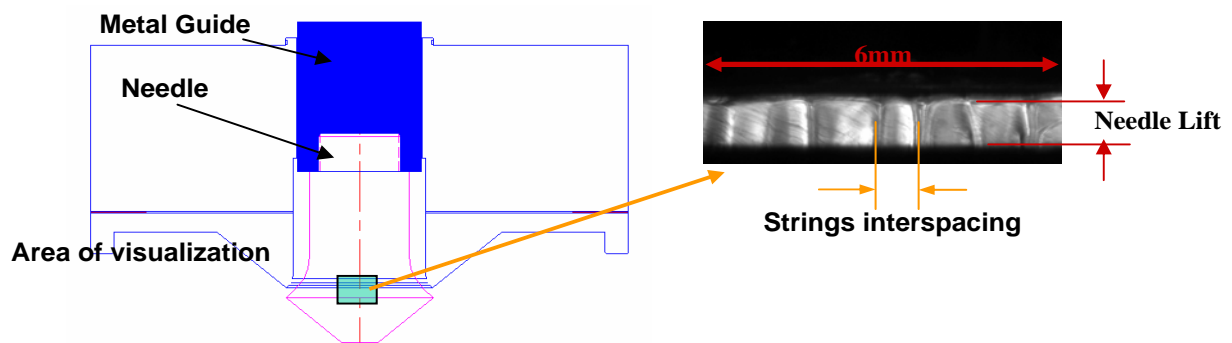

Figure 12 Visualization of the flow in the gap between the needle and its seat.

(a) 0.95 l/s, 4.96 m/s

(b) 1.25 l/s, 6.5 m/s

(c) 1.7 l/s, 8.9 m/s

Needle lift=0.93 mm

(d) 0.95 l/s, 8 m/s

(e) 1.25 l/s, 10.5 m/s

(f) 1.7 l/s, 14.3 m/s
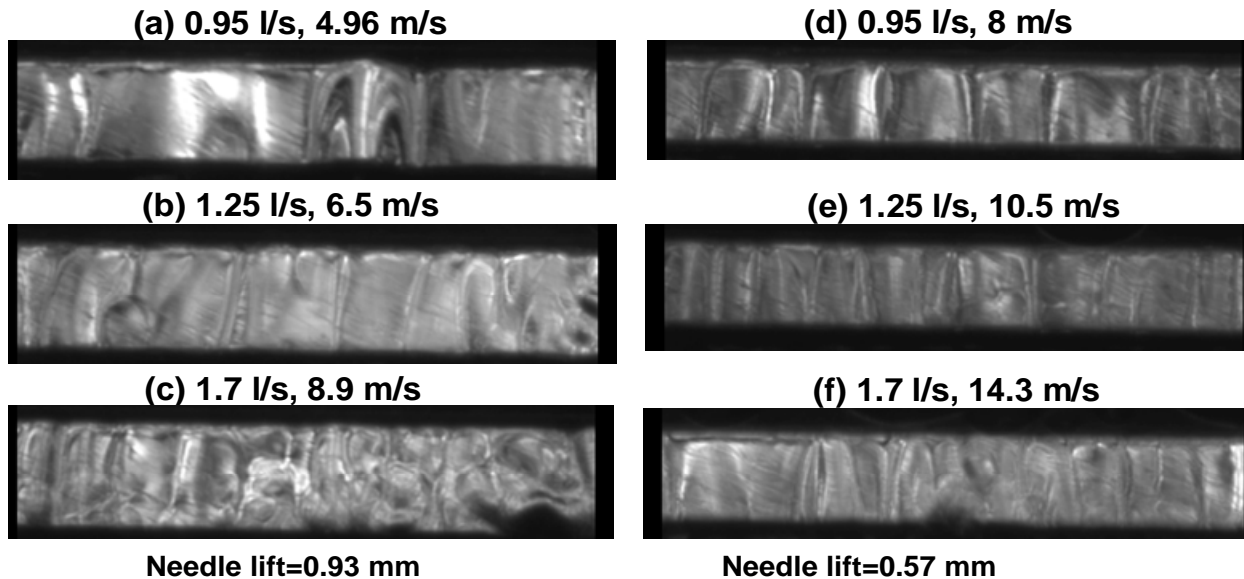
Needle lift=0.57 mm

Figure 13 Images showing the strings in the gap between the needle and its seat for different flow rates, injection velocities and needle lifts.

Figure 13 shows a sample of the flow structure images at three flow rates and two needle lifts. Although the mechanism of formation of the strings seems to be similar, the length scale of the whole structure becomes smaller as the liquid flow velocity increases. At higher flow velocities the strings structure becomes more complex as shown in Fig. 13(c). Comparison of the images in Figs. 13(c) and 13(f) for two needle lifts but at the same flow rate indicates that, despite the higher velocity through the nozzle at the lower lift, the strings structure under these conditions is well defined. This may suggest that the appearance of this complex structure is related to the ratio between the needle lift and

strings interspacing distance defined in Fig. 12. If the needle lift becomes larger than the strings interspacing distance, the probability of having such a complex string structure increases. The complex structure is associated with the formation of spanwise waves which are caused by Kelvin-Helmholt instability and are superimposed on the main streamwise filaments as explained by Mansour and Chigier (1991). The growth of these waves gives rise to the type of distorted waves emulating the corrugated surface associated with internal flow. These structures are similar to those presented by Arai and Hashimoto (1985) and more recently, by Carvalho et al. (2002).

The number of strings within the viewing window of 6 mm width was counted based on 20 images for each flow condition and an the average interspacing distance between two adjacent filament was calculated and presented in Fig. 14. The results show that the average strings interspacing distance decreases linearly with increasing injection velocity while the effect of needle lift on strings interspacing was negligible. Thus, the main factor affecting the strings interspacing is the injection velocity or injection pressure. It should be noted that the rate of reduction of strings interspacing with velocity presented in Fig. 14(a) is true only for the measured range and cannot be extrapolated to higher injection velocities. It can thus be anticipated that there is a limit beyond which the injection velocity has no effect on strings spacing since the same strings have been observed in the real size injector where injection velocities are much higher.

Results of Carvalho et al. (2002) using a liquid film with air impingement showed a slight change in the strings spacing with increasing injection liquid velocity provided the air velocity is kept constant. However, increasing the air velocity showed a significant reduction in the strings spacing. In the present set of measurements, there is no air impinging on the liquid film although there is always entrained air whose speed increases proportionally to the fuel flow velocity.

In order to understand more the dynamics of the strings and their method of formation, a high speed camera has been employed. Different recorded frequencies have been selected and the flow was visualized for different flow rates and valve lifts within the range presented in Fig. 13. By examining the different images from both the CCD camera and the video recorder of the flow, it was possible to propose a mechanism for the formation of these strings.
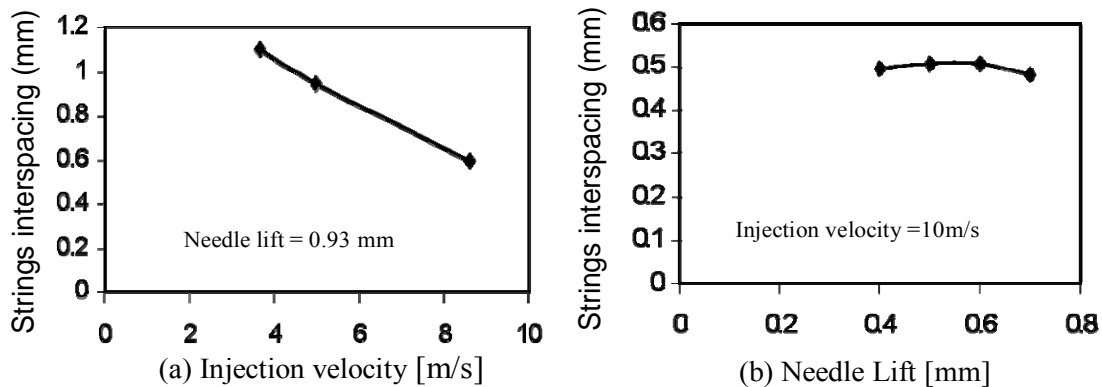

(a) Injection velocity [m/s]   (b) Needle Lift [mm]

Figure 14 Variation of strings spacing as a function of injection velocity and needle lift.

As the liquid flow emerges from the nozzle at high velocity, atmospheric air is entrained towards the nozzle exit with relatively high velocity and momentum [9]. The impact of the aerodynamic force on the emerging liquid initiates a distortion on the outer surface of the liquid film. When the magnitude of this instability reaches a critical point, the first break-up takes place in regions where the liquid film is very thin. At the same time, the force due to the liquid surface tension contracts the liquid where the liquid sheet is thickest, thus forming streamwise strings. This final formation of the strings structure that appears on the liquid film exiting from the nozzle is therefore the result of the balance of these forces. The structure of these interconnecting strings could be schematically presented in Fig. 15. The exact shape of the surface profile is governed by the interaction between the

aerodynamic force, the surface tension force and the momentum of the liquid flow as expected by the continuity equations. Fig. 16 shows the CFD calculation performed by Tonini [10], of the air flow that acts as a cross-flow to the injected fuel near the nozzle exit and of the presence of a strong recirculating air flow with velocities of the order of 70 to 130 m/s impacting on the surface of the emerging fuel film with exit velocities of around 300 m/s.

The fact that the strings interspacing is independent of the liquid flow Reynolds and Weber numbers supports the argument that these strings are produced as a result of the entrained air flow. In fact isolating the entrained air during the injection of the liquid could be a way to prove that approach if this is possible experimentally. It will be future work to correlate these strings spacing with the break-up frequency which may allow prediction of the break-up length and droplet size from the primary atomization process and scaling of the results down to the real size injector.
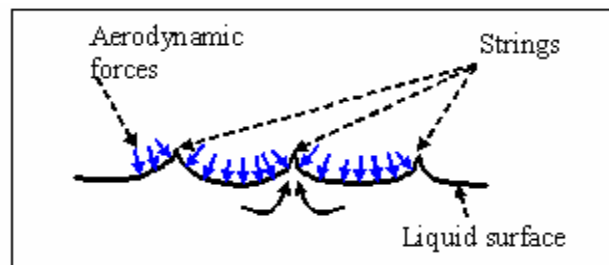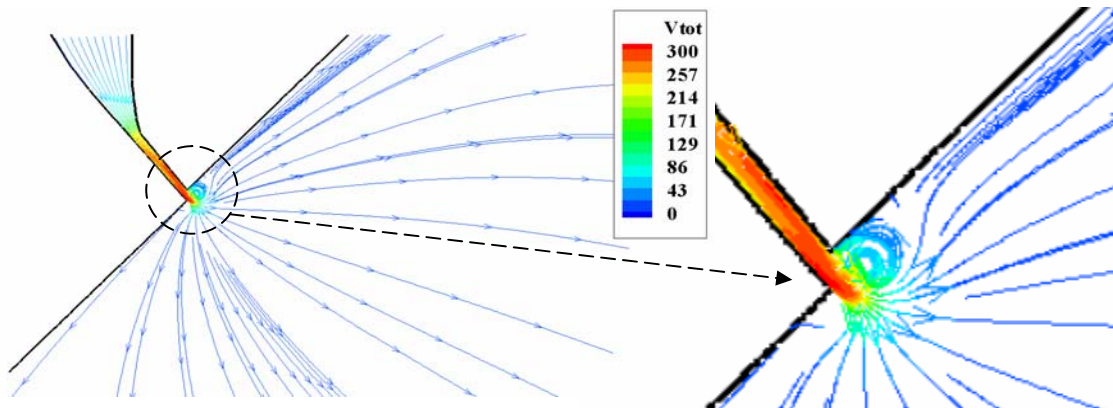

Figure 15 Liquid displacement to form strings.

Figure 16 Air flow streamlines close to the nozzle exit for an injection pressure of 250 bar and atmospheric back-pressure [10].

4. Conclusions

The internal nozzle and near nozzle exit flows of an enlarged transparent model of an outwards opening injector were investigated for different flow rates and needle lifts under steady state flow conditions. A high resolution CCD camera, a high speed video camera and LDV were employed to visualize the nozzle flow characteristics and quantify the tangential velocity distribution. The following are the main findings:

1- The internal flow above the valve seat comprised four separated jet flows originating from the square cross-section needle guide and four pairs of counter-rotating vortices with each pair bounded in-between two adjacent jets. The counter-rotating vortices are highly unstable in both longitudinal and circumferential directions with the latter transmitted to the exiting spray and causing a circumferential

oscillation of the same frequency. Similar flow pattern and instability was observed at all flow rates and valve lifts.

2- Magnified images of the flow just outside the nozzle exit revealed a streamwise interconnecting string-type spray structure as the liquid film emerges from the exit passage and interacts with the air. The formation of these strings can be due to the off-balance between the liquid jet dynamic force, the surface tension force and the aerodynamic force impacting on the liquid film through air entrainment.

3- The interspacing between the strings was found to be linearly related to injection velocity and almost independent of the needle lift within the range of examined operating conditions.

4- Tangential liquid velocity measurements obtained with LDV confirmed the existence of low speed rotational oscillations of the flow as a result of internal geometry of the injector; the dominant frequencies of these oscillations were found to be linearly related to the Reynolds number of the exit liquid flow.

References

[1] Fraidl G., Piok W., Fürhapter A., Sikinger H. and Pinter A., "The potential of next generation gasoline direct injection technologies", Associazione Tecnica dell'Automobile, 56:5-17, 2003.

[2] Iwamoto, Y., Noma, K., Nakayama, O., Yamauchi, T., and Ando, H. "Development of gasoline direct injection engine." SAE Paper 970541, 1997.

[3] Xu, M. and Markle L.E. (1998) "CFD development of spray for an outwardly opening direct-injection gasoline injector" SAE Paper 980493, 1998

[4] Gavaises, M. and Arcoumanis C. "Modelling of sprays from high pressure-swirl atomizers" Int. Journal of Engine Research, Vol. 2 (2), pp. 95-118, 2001.

[5] Mitroglou, N., Nouri, J. M., Gavaises, M. and Arcoumanis, C. (2006) Spray characteristics of a multi-hole injector for direct-injection gasoline engines. Int. Journal of Engine Research, Vol. 7(3), pp. 255- 270.

[6] Mansour, A. and Chigier, N. "Dynamic behavior of liquid sheets" Phys. Fluids A, Vol. 3(12) pp. 2971-2980, 1991.

[7] Arai, T. and Hashimoto, H. "Disintegration of a thin liquid sheet in a concurrent gas stream" ICLASS-85, London, UK, 9-10 July, 1985

[8] Carvalho, I. S., Heitor and Santos, D. "Liquid film disintegration regimes and proposed correlations", Int. J. of Multiphase flow, vol. 28, pp. 773-789, 2002

[9] Berthoumieu, P. and Lavergne, G. "Video techniques applied to characterization of liquid sheet break-up", J. of Visualization, Vol. 4, No. 3, pp. 267-275, 2001.

[10] Tonini, S., "Multi-phase flow modelling of fuel injection processes in direct injection diesel and gasoline engines", PhD Thesis, The City University London, UK, 2006.